Influence of Individual Ribcage Shape Variability on Occupant Rib Fracture Risk

Karl-Johan Larsson, Johan Iraeus, Bengt Pipkorn, Sven Holcombe

Abstract Human body models (HBMs) offer the potential to predict injury risk across broad populations. Adapting baseline HBM geometry to different body shapes, however, is often done using statistical shape models based on age, sex, height and weight, which generally explain less than half of the population variability. Here we explore that residual ribcage shape variability within a subpopulation (average height/weight males) and its influence on rib fracture risk using the SAFER HBM in simulated frontal and side impacts. Principal component (PC) analysis of rib centroidal path curves was used to define the overall ribcage geometry variation from 89 males, and the SAFER HBM was then morphed along each PC dimension. Six PCs described 90% of the geometric variance, with the first two PCs (generally representing variations in rib angles and lengths) describing 75% of this variance and having the largest influence on frontal and side impact rib fracture risk. Changing rib angles or rib lengths altered the left-right balance of seatbelt loading in the frontal impact, increasing rib fracture risk. In side impacts, rib fracture risk increased with increasing ribcage width. Ribcage shape models should consider parametrisation beyond broad demographic variables to represent variability critical for rib fracture risk.

Keywords Human body modelling, ribcage geometry, rib fracture risk, vehicle safety.

I. INTRODUCTION

While developments in vehicle crash safety over time have resulted in reduced risk of many occupant injuries, the risk of rib fractures has not been reduced when comparing pre and post-2009 vehicles [1-2]. Thus, fractured ribs remain a common injury outcome in vehicle crashes [2-3]. The risk of occupant thoracic injuries and rib fractures generally increase with increasing age, increasing body mass index (BMI) (weight divided by height squared (kg/m^2)) and is greater for females than for males [2][4-5]. This indicates a need to further consider occupant variability in vehicle and restraint system design to provide optimal thorax protection for the individual occupant.

Occupant injury risk has traditionally been evaluated using anthropometric test devices (ATDs) in physical and virtual vehicle crash tests. ATDs are simplified representations of the human anatomy and injury prediction is limited to a regional risk assessment, such as overall chest injury risk. This evaluation may be too simplistic to reveal the rib fracture injury mechanisms and can thus hinder identification of effective preventive measures. Finite element human body models (HBMs), such as THUMS, GHBMC and SAFER HBM [6-8], have gained widespread use in vehicle safety research and development and are used as complements to ATDs in occupant injury risk evaluations. Using HBMs with each rib modelled in detail, rib fracture risk can be evaluated at the tissue level by means of physical measurements related to fracture [9], providing insights to injury mechanisms.

Traditionally, HBMs are based on medical geometrical data representing a single individual with a fixed thorax shape and therefore require modification to represent occupant variability. Such modifications have included degrading material mechanical properties, reducing rib cortical bone area, and modifications of ribcage geometry to represent trends of increasing age or sex differences in the thorax of HBMs [10-12]. To facilitate representation of a wider range of occupants, a parametric HBM morphing method has been developed [13]. Using this method, a baseline HBM is morphed (re-shaped) to conform with statistical human-shape geometry models of body surface, pelvis, femur, tibia, and ribcage based on four demographic input parameters (sex, age, height, and BMI). Parametric HBM morphing enables evaluation of how anthropometric trends influence injury risk predicted with an occupant model [14]. However, the statistical ribcage geometry model used for parametric HBM morphing is only capable of representing 51% of the total variability of ribcage geometry among the 101 individual ribcages it is based upon when parametrised w.r.t the four demographic parameters mentioned above [15].

K. Larsson (karl-johan.larsson@chalmers.se) is a PhD student in Vehicle Safety at Chalmers University of Technology, Gothenburg, Sweden, and a Research Engineer at Autoliv Research in Vårgårda, Sweden. J. Iraeus is a Researcher at Chalmers University, Gothenburg, Sweden. B. Pipkorn is Adjunct Professor at Chalmers University, Gothenburg, Sweden and Director of Simulation and Active structures at Autoliv Research, Vårgårda, Sweden. S. Holcombe is a Researcher at the International Center for Automotive Medicine, University of Michigan, Ann Arbor, USA.

Another study of ribcage geometry, [16] used CT-scan data from 1,024 individuals to create another statistical shape model describing rib centroidal path shape and rib orientation relative to the spine as centroidal path curves with associated orientation parameters. Multivariate regression models based on sex, age, height, and weight explained 0-52% variability in rib curve shape and orientation parameters. Evidently, there are substantial inter-individual variations in ribcage geometry beyond those explained by trends due to age, sex, height, and weight. Hence, each ribcage shape produced by these statistical models is an expected average for individuals matching the input parameters, but the substantial regression model residuals indicate that a wide range of ribcage shapes exists.

As previous studies have used statistical trends in ribcage shape based on demographic parameters when modifying HBMs to represent occupant variability, the potential influence of the residual variability on occupant rib fracture risk predictions with HBMs is not known. In other words, given, for example, a subpopulation of average sized males, how would the shape of the ribcage vary within this subpopulation, and moreover, how may this variation influence occupant rib fracture risk predictions with an HBM?

Characterising the variability in ribcage shape within a subpopulation and to identify which, if any, ribcage shape variations have a substantial influence on HBM rib fracture risk predictions are the topics of this study. To evaluate influence on rib fracture risk predictions due to ribcage shape variations, the shape variations must first be geometrically represented in the HBM, which can be accomplished using mesh morphing. However, mesh morphing requires a geometric description of the target configuration.

For human shape modelling, principal component analysis (PCA) has been used as a method to create parametrised geometric descriptions of shape variability [15][17-18]. Using PCA, the geometrical shape data, often consisting of several point coordinates, with X,Y, and Z-components for each sampled individual, is linearly transformed into a new basis consisting of ordered and orthogonal vectors, i.e., the principal components (PCs). The first PC is in the direction of maximum variance, the second PC is in the direction of second to most variance, etc. Thus, for modelling variability trends within a sample, PCA offers an effective parametrisation that can generate geometric targets for morphing.

Further, studying how model parameters sourced from some population may influence a certain model output (here, rib fracture risk due to PC-based ribcage shape changes) is not always straightforward due to possible interaction effects. Still, from an occupant safety perspective, it is desirable to quantify what trends in ribcage shape (or here, PCs) are most influential for rib fracture risk. Such knowledge can be used in the development of future human shape models intended to represent the human variability in vehicle safety evaluations. Variance-based sensitivity analysis decomposes the variance of model output into fractions that can be attributed to the model input parameters using first order and total sensitivity indices [19-20], thus quantifying parameter influence on the output. The first order index quantifies the average influence on the variance of the output from varying a parameter according to its distribution, for all possible combinations of input parameters. The total sensitivity index for a parameter contains the first order effect and additionally all interaction effects.

The aims of the current study are to first characterise the variability in ribcage shape within a subpopulation, and secondly, to determine which shape variations substantially influence occupant rib fracture risk in frontal and near-side lateral impacts through variance-based sensitivity analysis. We address these two aims using a rib shape PCA applied to HBM geometry followed by a variance-based sensitivity analysis in simulated frontal and near-side lateral impacts.

II. METHODS

A brief outline of the analysis steps and data sources is provided here, with methodological details then expanded upon in subsequent sections. The SAFER HBM v10 (SHBM) [8] was the HBM chosen as the baseline FE geometry for this study as it has a ribcage model validated for predicting rib strain, and rib strain-based fracture risk, in various impact configurations [9][21-22]. Ribcage shape variability was characterised through PCA of ribcage geometrical data obtained from male live-subject CT scans (n=89) chosen to closely match the SHBM in terms of height and weight. The ribcage and surrounding parts of the HBM were morphed according to ribcage shape variations described by PCs. Each morphed SHBM was seated as a driver in a generic vehicle interior model [9][23] with seatbelt webbing routing applied according to the shortest path over each morphed HBM torso using the Primer pre-processor (Primer 17.0, Oasys Ltd.). Simulations of frontal and near-side lateral impacts were then performed using LS-Dyna (R9.3.1 MPP, 16 CPUs, LSTC, Livermore, California, United States), with sensitivity analyses according to [24] performed for each crash scenario to understand the influence of varying the ribcage shape on the risk of sustaining two or more fractured ribs (NFR2+). NFR2+ risk was calculated using a strain-based and age-adjusted probabilistic method [25-26]. The age was fixed to 45 years in the risk evaluation. The inputs to the probabilistic fracture risk calculations were the peak first principal strains, measured in the neutral element layer, from each of the HBM ribs cortical bone.

Ribcage Shape Variability

Parametric curves describing the rib centroidal path (a curve passing through the centroid of consecutive rib cross-sections) were used to describe rib- (a single curve) and ribcage shape (the collection of curves from a subject) [16][27-28]. Subjects used here were a subset of the sample in [16], in which rib centroidal path curve parameters were fitted to thoracic CT-scan data obtained at the University of Michigan (under IRB approval HUM00041441). Scans were from adult patients admitted to a trauma centre, and scans showing skeletal abnormalities were excluded, as were fractured ribs [16]. Among individuals with rib curve parameters fitted to their ribs, a subpopulation with limited height and weight and a single sex were selected by the inclusion criteria: Sex=Male, Age >18 years, height in range 1.72-1.82 m and weight in range 72-82 kg. This resulted in a sample of n=89 males (descriptive statistics in TABLE A I) close to the SHBM size in terms of height and weight (177cm, 77kg).

Initial analysis showed that there was a large length variation in the 12th rib (the most inferiorly located rib) which resulted in a PC mainly describing this length variation. As the 12th rib is rarely fractured in injured vehicle occupants [29-30], the 12th rib was excluded from the PCA in favour of prioritising PCs describing shape variations to the complete ribcage structure.

Out of the 89 individuals in the sample, 57 had fitted curve parameters for all rib levels. In total 6% of the ribs were missing due to not having curve parameters. Among missing ribs, 48% were the most superior and inferior ribs. To obtain more complete ribcage shape descriptions for all 89 individuals, first, left-right symmetry was assumed. Left rib curve parameters for each rib level were taken as the average of left and right, or only the left or right if one side was missing, or, assigned as missing if neither side had fitted parameters. Following this step, 66 individuals had parameters for all left ribs (level 1-11), and in total 5% of the left ribs were missing parameters. Secondly, the still missing rib curve parameters were imputed using the method of trimmed scores regression, which uses known data to construct a PCA-based regression model to predict the missing data [31-32], resulting in complete rib curve parameter sets for all 89 individuals.

As the rib curves were originally fitted to ribs in supine CT scans, all rib curves were re-positioned to the seated configuration of the SHBM. Supine-to-seated translation and rotation offsets for each rib level were determined by manually repositioning a set of left side rib curves created for an average male, to align with the ribs of the average male ribcage in the SHBM. The average male rib curves were created for a male of 1.77m, 77kg and 50 years of age, using a regression model predicting rib curve parameters [16]. The translation and rotation offsets for each rib level were recorded, and then applied to each corresponding rib curve from all sampled individuals. Thus, for an individual with rib curve orientation coinciding with the regression predictions for an average sized male, the rib curves will be aligned with the ribs in the SHBM ribcage. Any deviation of rib curve orientation relative to the regression predictions will likewise be a deviation of the same magnitude and direction relative to the seated SHBM rib orientation. As the SHBM ribcage shape and rib orientation relative to the spine are based on averaged male data [21][33], it represents a ribcage with average shape and rib orientation.

Ribcage Shape Parameters from PCA

The set of rib curves from all individuals in the sample were discretised by generating 101 equidistant points along each curve. The X-, Y- and Z-coordinates of these points were the input for PCA, i.e., 89 observations of 1111*3 variables (11 left ribs (12th excluded), 101 points per rib, three coordinates per point). PCA was performed using MATLAB, Statistics and Machine Learning Toolbox (R2017b, The MathWorks, Inc. Natick, Massachusetts, United States). The resulting PCs were ordered in percentage of variance explained. Standard deviation (SD) of the individual scores for the PCs were calculated. Here, individual scores refer to an individual's coordinates in the new PC-basis. Rib curve points for all 11 left ribs were then re-created using *one PC at-a-time* from the parametric expression in Equation 1:

$$\boldsymbol{C_i}(s) = \boldsymbol{\mu} + \boldsymbol{P}_i^T \sigma_i s \ [mm] \qquad (Eq. 1)$$

where, $\boldsymbol{C_i}$ is a vector of rib curve point coordinates, $\boldsymbol{\mu}$ is the average point coordinates, $\boldsymbol{P}_i$ is the ith principal component, σ_i is the sample SD of scores for the ith principal component and s is a scaling coordinate. Thus, e.g., i=1 and s=2 the resulting rib curve point coordinates represent the ribcage shape for +2 SD of score for PC 1.

Representing PCA-based Shape Parameters in HBM Through Morphing

The expression in Eq. 1 was used to generate points along left rib curves for the different PCs and levels of the scaling coordinate. The generated points were used as morphing targets to morph the SHBM ribs and torso in a five-step process.

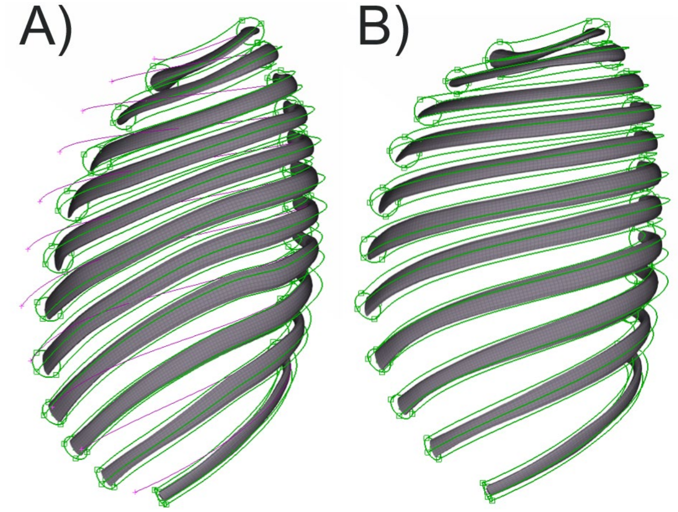

Fig. 1. A). Original left ribs 1-11 of SHBM in a lateral view. A cylindrical morph box (green) with rib centroidal path as centre encloses the elements of each rib. Centroidal path morph targets generated from PC 1 at +2SD (i.e., i=1 and s=2 in Eq. 1) seen as 3D splines (magenta). B). Ribs have been morphed by aligning each cylindrical morphbox to its target spline.

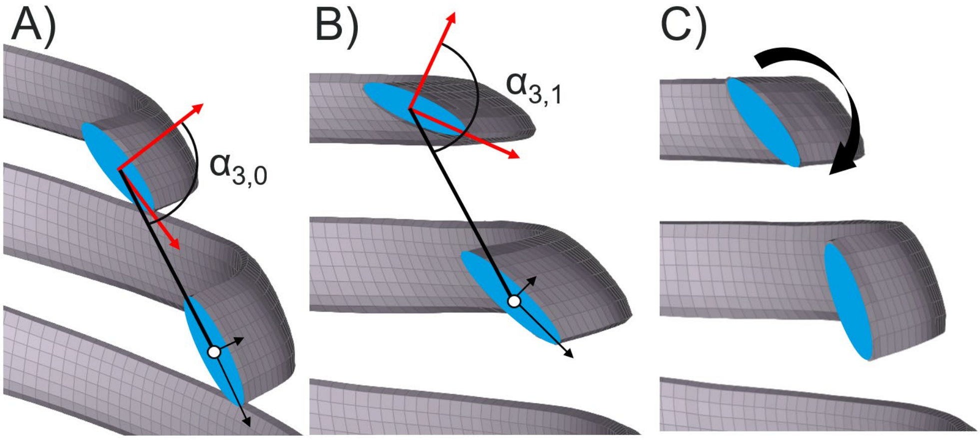

Fig. 2. Adjustment of cross-sectional twist along rib, demonstrated for the third rib. A). Orientation of anterior end cross-section (blue ellipse) relative the inferior rib before morphing as defined by angle $\alpha_{3,0}$. This angle is measured in a local 2D coordinate system defined by the major and minor axes of the rib cross-section at the anterior rib end. A line extending from the origin to the projection of the inferior rib cross-section centre defines the angle. B) The same angle measured again after morphing the ribs, resulting in $\alpha_{3,1}$. The difference of the two angle measurements was used to adjust the twist of the anterior rib cross-section. The amount of twist was linearly interpolated to 0 at the posterior end of the rib. C) Anterior end twisted to final configuration.

The first step was morphing of the left ribs. The rib morphing process is visualised in Fig. 1 and Fig. 2 and explained briefly in the following. Each individual rib was morphed to align its centroidal path to the new target centroidal path using a cylindrical morph box containing the elements of the rib (Fig. 1). Cylindrical morph boxes preserve cross-sectional dimensions while allowing the morphed structure to align itself along a specified target path. Here, the target path for each rib was a spline fitted to the corresponding rib curve points as obtained from Eq. 1. In the second step, the twist of the rib (how the rib-cross section is rotated relative its centroidal path) was adjusted. As the rib curves only described centroidal path shape, twist was not controlled for during centroidal path alignment with the target rib curves. To control twist adjustment, it was assumed that the elliptical cross sections of each morphed rib would have the same rotation relative to its inferior rib, as it did before the morphing (Fig. 2). Centroidal path alignment and twist adjustment was performed using the pre-processor Ansa (v19.1 Beta CAE Systems, Thessaloniki, Greece). In the third step, the morphed left ribs 1 through 11 were reflected to create morphed right ribs and the sternum was repositioned, first by a translation following the movement of the second rib pair, then by a rotation about an axis connecting the anterior ends of the morphed second rib pair. The angle of rotation was determined by the change of angle between a line connecting the centre points between the second and the sixth rib pairs and the vertical axis (Fig. 3).

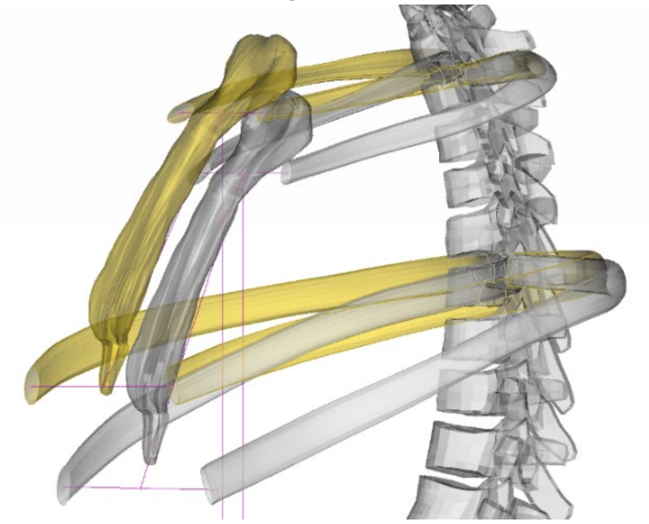

Fig. 3. Repositioning of the sternum using positions of the second and sixth rib pairs before (grey) and after (yellow) rib morphing. The purple straight lines demonstrate the pre- and post-rib morphing geometrical information used to reposition the sternum. A line connecting the second rib pair, a line connecting the sixth rib pair and lines connecting the midpoints of these lines, and a vertical line that the sternum angle is measured relative to.

Fourth, the mesh of costal cartilage, intercostal muscles and the 12th rib pair were morphed to align to the newly obtained rib shapes and sternum location, resulting in a morphed ribcage. In the fifth and final step, parts of the torso and the upper arms, surrounding the newly morphed ribcage, were morphed to adapt to the shape of changes of the ribcage. A MATLAB implementation of the radial basis function used for parametric HBM mesh morphing method presented in [13] was used in the fourth and fifth step.

The ribcage morphing resulted in a change of total volume of the thoracic region of the model. To avoid differences in torso mass between the morphed models, the density of soft tissue materials in the torso was uniformly scaled such that each morphed SHBM retained the mass of the original SHBM. For all morphed models, element quality (Jacobian ≥ 0.5) was maintained in morphed parts and all HBM internal contact surfaces remained intersection free.

Parametric Sensitivity Analysis of Ribcage Shape

The SHBM was seated as a driver in a generic vehicle interior model [9], [23] that was used for two crash scenarios. They represented a frontal impact and a near-side lateral impact, that are common crash configurations in consumer safety testing, with a high risk for occupant thoracic injuries in real-world crashes [3]. In both crashes, the delta-velocity was chosen such that the HBM with the average ribcage shape from the PCA predicted approximately 50% risk for NFR2+. The frontal impact crash scenario had a delta-velocity of 45 km/h. The seatbelt had retractor pre-tensioning and load limiting (3.5 kN), and the steering wheel airbag had a peak pressure of 25 kPa in the frontal impact. In the near-side lateral impact case the seat mounted airbag had a peak pressure of 55 kPa and the inflatable curtain airbag had a 60 kPa peak pressure. The lateral impact had a delta-velocity of 24 km/h, and a peak door intrusion of 88 mm measured at the armrest of the door panel. The respective vehicle and accident parameters were held constant while ribcage geometry was varied in all frontal and lateral impact simulations.

The sensitivity analysis method presented in [24] was adopted, and is explained briefly for completeness. In the general sense, a model output, Y, depends on its input parameters, $X = [x_1, x_2, \ldots, x_n]$, through some function, $Y = h(X)$. Each parameter is considered a random variable with some associated density distribution. Variance-based sensitivity analysis utilises the variance decomposition of the output [34-35] (Eq. 2):

$$V_Y = \sum_{i}^{n} V_i + \sum_{i}^{n} \sum_{j>i}^{n} V_{ij} + \ldots + V_{ij\ldots n} \qquad (Eq. 2)$$

Where V_i is the partial variance of Y due to varying parameter x_i, V_{ij}, is due to the interaction of x_i and x_j and so on. The primary, or first order, sensitivity index is $S_i = \frac{V_i}{V_Y}$, which represents the main, average effect contribution (disregarding interactions) of varying x_i, over all possible combinations of the other input parameters. The total sensitivity index, S_{Ti}, accounts for the total contribution to V_Y, due to x_i, including all higher order interactions [19-20]. In practice, Monte Carlo methods sampling many points X are used to compute the sensitivity indices, but for models where a function evaluation has a non-trivial time cost (here, approximately 6 hours), this approach is not feasible. Instead, the approximative method presented in [24], based on a multiplicative dimensional reduction method (M-DRM) was used to calculate the S_i and S_{Ti} sensitivity indices. This method was chosen for its computational efficiency, obtained from the assumption that the model output around a point in the input-space, the cut-point: $X = C = [c_1, c_2, \ldots, c_n], h_0 = h(C)$, can be decomposed into a set of one-dimensional functions, through M-DRM (Eq. 3):

$$h(X) \approx h_0^{1-n} \cdot \prod_{i=1}^{n} h_i(x_i, C_{-i}) \qquad (Eq. 3)$$

Where $h_i(x_i, C_{-i})$ is a function of x_i and C_{-i} is C with c_i excluded. From this assumption, it follows that computing one-dimensional integrals, through e.g., Gaussian quadrature, provides sufficient information to calculate the sensitivity measures S_i and S_{Ti}. For a function of n parameters and a quadrature rule of N_{GP} Gauss points, at most $n \cdot N_{GP}$ function evaluations are needed (see [24] for details).

Here, the cut-point, or the baseline case which all ribcage shape parameters were varied about, was selected to be with the average ribcage shape from the PCA ($s = 0$ in Eq. 1). The first PCs together representing more than 90% of ribcage shape variability were used as ribcage shape parameters. The parameters were varied as normally distributed within ±2 SDs of the respective PC sample scores ($s \in [-2, 2]$ using Eq.1), and five-point ($N_{GP} = 5$) Gauss-Legendre quadrature was used. The range of ±2 SDs was chosen because more extreme values resulted in degraded mesh quality in the 3D-intercostal muscle elements when morphing.

Changes in Rib Strain due to PC Based Ribcage Shape Changes

As all ribcages were morphed versions of the same mesh, resulting rib strains could be compared at the element level. The rib cortical bone first principal strain obtained in the first Gauss point evaluation was subtracted from the corresponding result in the last Gauss point evaluation for each PC. These strain differences then corresponded to how the strain within each rib changed when the ribcage shape changed between these extremes, which could indicate why the NFR2+ risk changed. The strain differences were calculated and visualised on the average ribcage geometry using the post-processor META (v19.1 Beta CAE Systems).

III. RESULTS

Ribcage Shape Parameters from PCA

The variance explained and the score SD for the first ten principal components is shown in TABLE A II, Appendix A. The first six principal components together described more than 90% of the variance in the rib centroidal path geometry for the 89 males. The first two PCs alone described more than 75%. The following PCs carried less information, with the third describing 5% and PCs 4 through 6 representing 4%, 3%, and 2% of the variance, respectively.

Morphing HBM to Rib centroidal Path Targets

The SHBM ribcage (including ribs, costal cartilage, and sternum) morphed to ±2 SDs of sample score for the first six PCs is shown in Fig. 4. The main shape effect of PC 1 is a variation of rib angles in the sagittal plane. Additionally, as the ribs rotate superiorly, their anterior ends move laterally, creating a wider ribcage. PC 2 describes variation in the end-to-end span length of the ribs with related changes in rib curvature. Shorter ribs had more curvature, and the ribs were straightened out when length increased. PC 3 mainly describes a variation in rib cage width. While less evident on static images (animated demonstrations of shape effects can be found in [36]), the fourth

PC also describes a variation in rib cage width, in form of trapezoidal-like variation (wide/narrow at top or bottom). PC 5 describes a variation in the pitch of the rib path from spine to sternum (high or low at the posterior region) and PC 6 describes a variation in spacing between consecutive ribs.

In Fig. 5 the SHBM upper body as morphed to adapt to shape changes from PC 1 is shown.

Fig. 4. SHBM ribcage as morphed to s = -2 (orange) and s = +2 (pink) SDs of sample score for the first six PCs. Top row is a superior-inferior view, bottom row is a lateral view. Left to right is PC 1 to PC 6.

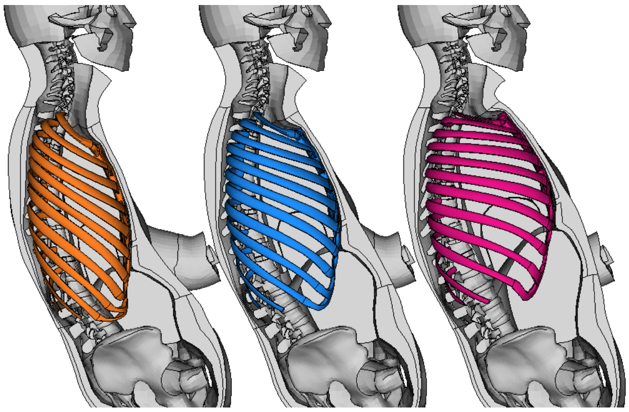

Fig. 5. SHBM with ribcage morphed to PC 1, with parts removed from visibility to show rib cage and surrounding parts. Left, middle and right represents s=-2, s=0 (mean ribcage shape) and s=2 SDs of score for PC 1, respectively.

Sensitivity Analysis Results

All simulations completed successfully (no error terminations). The kinematics of the SHBM in the cut-point evaluation (s=0) in the two crash scenarios is shown in Fig. A 1 (Appendix A).

Sensitivity index and total sensitivity indices are shown in Fig. 6. For frontal impacts, varying rib angles (PC 1) and rib end-to-end span length (PC 2) were the most influential shape changes for NFR2+ risk, according to primary and total sensitivity indices. The contributions of the remaining PCs to the variability in NFR2+ risk is smaller. In lateral impacts, varying rib end-to-end span lengths (PC 2) was the major contributing factor to NFR2+ variability, followed by variations in rib angles (PC 1).

The risk of NFR2+ obtained in each evaluated point for the respective PCs is shown in TABLE I for the frontal and lateral impacts. The risk in the cut-point, i.e., with the average ribcage shape, was 51% for both impact configurations. In the frontal impact, the variation in rib end-to-end lengths (PC 2) changed NFR2+ risk the most. The change of risk was 41%-units, and the maximum risk was 92% for s = 1.81. PC 1 produced greater changes in risk for more moderate ($s = \pm 1.08$) PC scores compared to PC 2 (TABLE I), which had a greater impact on rib fracture risk variability in the subpopulation, according to the sensitivity analysis (Fig. 6).

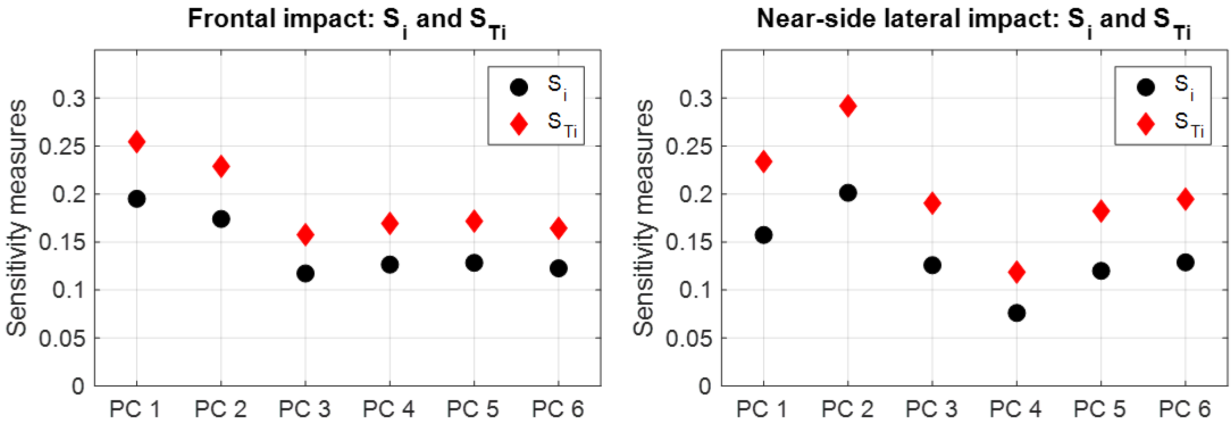

Fig. 6. Sensitivity indices S_i and S_{Ti} for frontal (left) and lateral (right) impacts. PC 1: rib angles, PC 2: rib lengths, PC 3: ribcage width, PC 4: trapezoidal width, PC 5: rib pitch, PC 6: rib spacing.

In the lateral impact, the variation in rib angles (PC 1) and the variation in rib end-to-end length (PC 2) both changed the risk by 50%-units over the range of evaluation (TABLE I). The NFR2+ risk also increased with an increase in ribcage width (PC 3), increased height of posterolateral rib regions (PC 5) and decreased spacing between consecutive ribs (PC 6). Varying ribcage shape according to PC 4 had the least influence on NFR2+ risk in the lateral impact.

TABLE I

RISK OF NFR2+ (%) FOR PC-SHAPE CHANGES IN EVALUATED SCALING COORDINATES, S, (SCALED GAUSS COORDINATE CORRESPONDING TO NUMBER OF STANDARD DEVIATIONS OF CORRESPONDING PC SCORE) AND RANGE OF RISK OBTAINED. *PC 1: RIB ANGLES, PC 2: RIB LENGTHS, PC 3: RIBCAGE WIDTH, PC 4: TRAPEZOIDAL WIDTH, PC 5: RIB PITCH, PC 6: RIB SPACING.*

Parameter Name	s=-1.81	s=-1.08	s=0	s=1.08	s=1.81	Range
		Frontal impact				
PC 1	64.0	61.0	50.8	76.4	77.0	26.2
PC 2	63.5	59.3	50.8	62.9	91.6	40.8
PC 3	54.4	52.1	50.8	49.4	51.5	5.0
PC 4	56.6	54.4	50.8	59.5	53.8	8.7
PC 5	49.5	47.0	50.8	56.4	59.2	12.3
PC 6	58.2	55.7	50.8	56.4	54.9	7.5
		Near-side lateral impact				
PC 1	26.0	45.3	51.0	72.8	76.8	50.9
PC 2	89.9	78.3	51.0	39.2	42.2	50.6
PC 3	39.1	45.3	51.0	66.0	80.9	41.8
PC 4	52.0	47.9	51.0	51.6	47.9	4.2
PC 5	37.9	42.7	51.0	61.9	77.6	39.8
PC 6	54.6	53.3	51.0	76.3	72.2	25.5

Changes in Rib Strain due to PC Based Ribcage Shape Changes

The change in rib strain (1st principal) due to shape changes from PC 1 in the frontal impact is shown at time T=96 ms in Fig. 7. The difference in strain indicates an increased loading of the left upper ribs (levels 3-5), and a decreased loading of the right mid ribs (levels 6-8), as the ribs angled superiorly with increasing score (s-coordinate) for PC 1. In Fig. A 2 the change in strain at time T=95ms, due to changing ribcage shape according to PC 2 in the frontal impact is shown. For a ribcage with longer and less curved ribs (s=1.81), the strain increased in right side ribs (levels 5-9) and was decreased in left upper ribs (level 3-5).

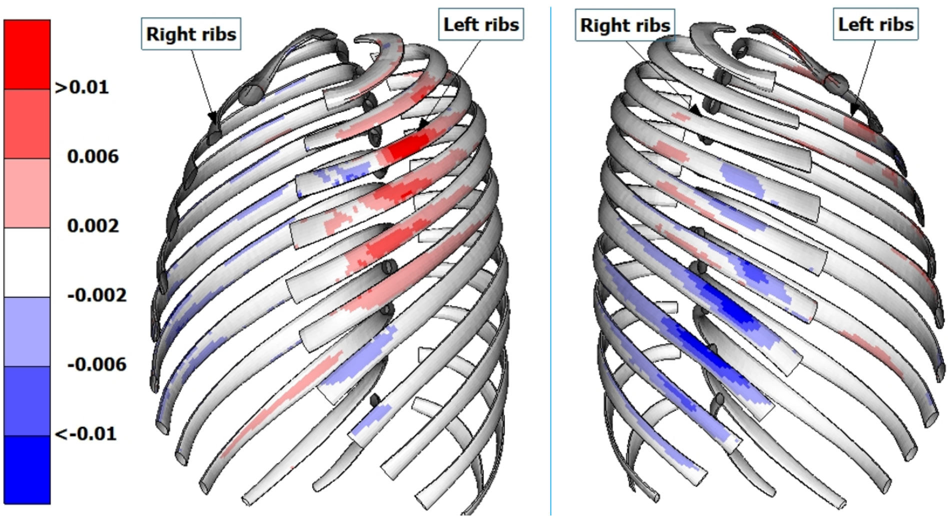

Fig. 7. PC 1, Frontal Impact, time T=96 ms: difference in rib cortical bone first principal strain. Views of the ribcage focusing on left and right ribs. Strains from s=-1.81 ribcage shape elementwise subtracted from s=1.81 ribcage shape. Red means difference is positive, blue means negative by 0.01 (1%-unit)

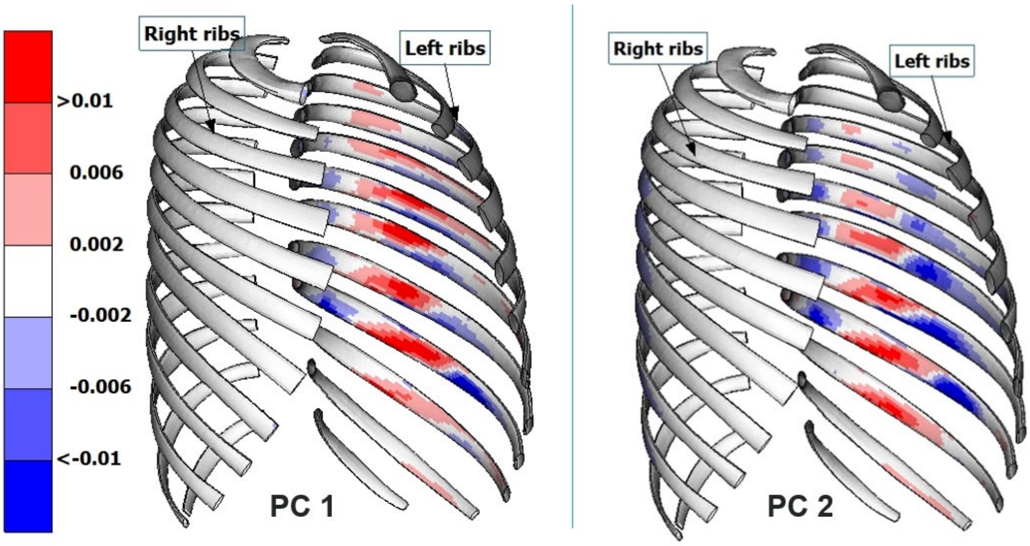

Fig. 8. Near-side lateral impact, time T=56 ms: difference in rib cortical bone first principal strain for PC1 (left) and PC 2 (right). Strains from s=-1.81 ribcage shape elementwise subtracted from s=1.81 ribcage shape. Red means difference is positive, blue means negative by 0.01 (1%-unit)

In the near-side lateral impact, the pleural side of the left (struck-side) ribs showed the most strain. The change of strain in the ribs between s=-1.81 and s=1.81 was similar for PC 1 and PC 2 (Fig. 8). Angling the rib upwards (PC 1) or increasing the rib length (PC 2) decreased strain levels in the lateral and posterior region of the ribs, and increased strain in the posterolateral region. This indicates that the focus of the loading from airbag and intruding vehicle structures moved posteriorly relative to the ribs in both cases. For ribcage width (PC 3) peak rib strain values increased with increasing width, which resulted in increased NFR2+ risk. A trend of increasing NRF2+ risk with increasing ribcage width (as measured between the two most lateral points on each ribcage) was observed across all PCs in the lateral impact (Fig. A 3, Appendix A).

IV. Discussion

The aims in this study were to characterise the variability in ribcage shape within a subpopulation and to determine which shape variations substantially influence occupant rib fracture risk in frontal and near-side lateral impacts through variance-based sensitivity analysis.

The variability of ribcage shape within a subpopulation consisting of n=89 close-to-average adult males was characterised through PCA. More than 75% of the variance in ribcage shape between otherwise similar males could be explained by two modes of shape variation: rib angles (PC 1), and rib end-to-end span length (PC 2) (TABLE A II). Age > 18 years was the only age restriction for the subpopulation, even though age has been found to be a statistically significant predictor for ribcage shape variations similar to those described by PC 1 and PC 2 in this study. Regarding angles of the ribs in the sagittal plane (PC 1), age trends have explained 4-10% of variability [10][16]. For rib end-to-end span length (PC 2), age explained 4-10% variability in male ribs [16]. Due to the low explanatory power of age found in previous studies, the influence of age on the shape variability described by PCs in this study can be considered small. Further, the amount of variance explained by PCs in this study does not correspond to the variance explained with other ribcage shape models due to difference in ribcage geometrical data and methods. For example, the parametric ribcage shape model in [15] predicts landmarks distributed along and around all ribs, and additional landmarks on the sternum and the thoracic spine through a regression model. That regression model is based on age, sex, height, and BMI, and has a reported R^2-value of 51%. Landmarks around the ribs, on the sternum and on the thoracic spine are additional features, introducing additional variability in [15], compared to the rib centroidal paths used for the current study.

The variability in rib angles (PC 1) and rib end-to-end span length (PC 2) found within the subpopulation of this study are indications of two modes of ribcage shape variations existing when controlling for sex, height, and weight. Even though the percent of variance explained is not directly comparable to previous studies, these two modes represent a large portion of variability in ribcage shape. Thus, to create a statistical ribcage shape model that represents the adult occupant population, considering parametrisation for these two modes of shape variation, in addition to demographic parameters, seems promising.

The ribcage shape variations used in the current study also had substantial effects on the resulting NFR2+ rib fracture risk (TABLE I). Among all shape variations represented by PCs, the parametric sensitivity analysis showed that PC 1 and PC 2, or rib angle and rib length variations, were the most influential for NFR2+ risk in both the frontal and the lateral impact scenario (Fig. 6). In the frontal impact, angling the ribs upwards (PC 1) or increasing rib lengths (PC 2) changed the levels of strain obtained in left or right ribs (Fig. 7 and Fig. A 2). Thus, both these shape variations affected the left-right balance of loading to the ribs. As the ribcage morphing was symmetric, and the steering wheel airbag had a symmetric shape, any asymmetry in chest loading can be attributed to differences in shoulder belt interaction. For both PC 1 and PC 2 morphed ribcages, the seatbelt crossed the sternum at approximately the same height in its initial position (Appendix A Fig. A 4 and Fig. A 5). However, changing the shape of the ribcage also changes how the shoulder belt wraps the torso, which appears to influence if loading becomes focused on the left- or right-side ribs. For both PC 1 and PC 2, the frontal impact NFR2+ risk increased when moving away from the average ribcage shape in any direction (TABLE I). It is not clear if this would be the case in another vehicle where seat belt anchorage locations would be different, for example. Still, it indicates that a balanced loading of the torso is important to minimise rib fracture risk, and that this balance is affected by ribcage shape variability.

In the near side lateral impact, changing the ribcage shape according to PC 1 and PC 2 resulted in similar change of strain within the ribcage. In both cases, when angling ribs upwards, or increasing rib lengths, strain was reduced in the lateral and posterior regions of the left side ribs while it increased in the posterolateral region (Fig. 8). Paradoxically, this resulted in increased NFR2+ risk for increased rib angles, but a decreased risk for increased rib lengths (TABLE I). Due to the way in which the NFR2+ risk is calculated by means of a non-linear, s-shaped, risk function [26], such results are, however, possible. For example, increasing the strain in a region within a rib that previously was at low risk of fracture due to low levels of strain, an increase of 1%-unit in rib strain does not contribute substantially to the fracture risk within that rib (and to the total NFR2+). If the strain changed in a region where risk was around 50% of fracture, a 1%-unit change in rib strain will substantially change the risk. Increasing rib angles or shortening rib lengths also increased ribcage width (Fig. 4).

A trend of increasing NFR2+ risk with increasing ribcage width was observed across all ribcage shape variations in the near-side lateral impact (Fig. A 3). Increasing the width of the ribcage reduces the initial gap between the occupant and intruding side structure. Thus, the resulting NFR2+ risks are confounded by both ribcage shape variations and the correlated variation in initial distance to the side structure. Further studies are needed to isolate the ribcage shape contribution to NFR2+ risk. Nevertheless, the varying rib angles and rib lengths influenced the NFR2+ risk the most, indicating a potential for reducing rib fractures by assuring that vehicle interiors and side impact protection systems are robust to such ribcage shape variations.

Previous studies using HBM simulations to investigate how ribcage geometry affects rib fracture predictions have used age-based trends to modify the ribcage geometry and have used simplified impact scenarios. Reference [10] rotated the ribs of the H-model HBM superiorly 7° (at the 9th rib) from the nominal rib cage geometry. This corresponded to a predicted age effect over 71 years of ageing. Reference [12] modified the shape of the midsize male GHBMC ribcage to correspond to a 30- and a 70-year-old male ribcage. The ribcage showed an average superior rotation of the ribs of 2.3° when aged by 40 years. In the current study, the corresponding change of the 9th rib angle over ±2 SDs of score for PC 1 was 23°, demonstrating that individual variability is stronger than the age trends used in previous studies. In [10], the age-based geometry change alone resulted in more strain-based rib fractures for a given deflection in table top belt loading scenarios. In [12], the aged geometry model predicted five additional rib fractures in a lateral rigid plate impact. While the current study used a vehicle environment to create loading conditions representative of real-life crashes there are no conflicting trends in results compared to the previous studies.

In this study, several methodological choices were made. The SHBM v10 was the occupant substitute used. This choice was motivated by previous validation of frontal and near side lateral impact NFR2+ risk predictions. The validations on the full HBM level were performed using SHBM v9. Updates of the SHBM to v10 includes a new average male pelvis model and remeshing of thoracic soft tissues with biofidelic material models for skin, adipose and skeletal muscle tissues. The ribcage mesh and material models were kept from v9 [8]. Validation of population NFR2+ risk predictions for various impact speeds in frontal and near-side lateral impacts were performed using the generic vehicle interior model used also for this study [9].

As the SHBM represents an average sized male, the subpopulation of this study was selected as average males. Although ribcage shape explained by sex, height, and weight, in statistical models leave large residuals, the effect on the expected ribcage shape is statistically significant (the expected average ribcage shape shifts with sex, height, and weight). Therefore, in this study, the average ribcage shape, and the variability around it can be considered typical for occupants of the height and weight represented by the SHBM. It should be noted that the error in predicting ribcage shapes is fairly constant over age, height and BMI, for both sexes in [15], indicating that the range of individual variability in ribcage geometry is similar for males and females. Evaluating the effects of variability in ribcage shape on rib fracture risk through HBM simulations in another subpopulation, e.g., small females, should preferably be done with an HBM representing the height and weight of that subpopulation.

The ribcage shape data consisted of rib centroidal path curves for the included individuals. While this data could be used to model ribcage shape variability based only on rib centroidal path shapes, no data for the relative position or geometry of the sternum, costal cartilage, or rib cross-sectional measures were included. Therefore, this study was performed without variability in sternal shape and relative position and with constant rib cross-sectional properties (more on cross-sectional variation in limitations below). The costal cartilage was morphed to connect the ribs and sternum. The twist of the ribs around the centroidal path was adjusted by an assumption of a similar twist orientation between adjacent ribs for all ribcage shapes. Adjusting the twist of the morphed ribs was necessary, as without adjustment the 3D-element intercostal muscle mesh was not able to connect neighbouring ribs without creating severely distorted elements. Further studies based on ribcage shape data including the sternum, costal cartilage, and rib cross-sectional twist and size information can reveal if individual variability in those geometric features also substantially affects rib fracture risk.

The approximate method in [24] for variance-based sensitivity analysis was used to quantify which PCA-based ribcage shape parameters had the largest influence on the NFR2+ risk prediction. The relatively expensive computational cost of full body HBMs in vehicle impact simulations, is often prohibitive when investigating influence of HBM parameters on different outputs. Some studies have varied one factor at-a-time between two different pre-selected levels [10][12], which cannot reveal non-linear interactions. Such methods also disregard the distribution of the parameter in the population, e.g., extreme results for unlikely parameter values, may potentially have less of an impact on rib fracture outcomes, for instance, than a small influence from a common parameter value. These limitations are overcome by variance-based sensitivity analysis, which can only be done explicitly for simple mathematical functions. Monte Carlo based methods for approximating the variance-based sensitivity measures require a large number of simulations. In [24], the approximative method used in this study is shown to be able to compute the sensitivity measures for several different functions with similar accuracy as state-of-the art Monte Carlo-based methods, provided a sufficient number of evaluation points are used for numerical integration. Here, five-point integration Gauss-Legendre quadrature was used (which integrates 9th degree polynomials exactly). Further, the accuracy of computed sensitivity indices depends on how well the M-

DRM (Eq. 3) assumption is fulfilled, which is not known for the current study. Therefore, the sensitivity analysis results are interpreted as indicative for which shape variations are most influential. Further studies are needed to confirm the applicability of the M-DRM method for HBM models in vehicle impacts.

There are several limitations with this study. Only one vehicle environment, with one initial posture of a midsize male HBM was used. Occupant size and position, restraint system and vehicle interior design are factors that are likely to contribute to the NFR2+ risk and potentially also to how this risk changes when the ribcage shape is changed. Further, we only studied one frontal and one lateral impact scenario. Real-life crashes occur in a range of impact scenarios with varying impact angle and severity. Moreover, only variability in rib centroidal path shape was studied here, while it is known that other mechanical aspects that can influence rib fracture risk vary between individuals. The rib cortical bone material parameters, e.g., Young's modulus, yield stress and yield strain, exhibits a declining trend with age, but also a substantial inter-individual variability [37-38]. In single rib anterior-posterior bending experiments, rib cross-sectional measures taken close to the fracture site (total cross-sectional area, cortical bone area, area moment of inertia) have significant correlations with displacement and force until fracture [39]. Rib cross-sectional properties are influenced by sex, but also show variability among individuals of the same sex [40]. It is likely that that varying rib material parameters and cross-sectional properties influence the predicted NFR2+ risk in HBM occupant simulations. Evaluating the effect of individual variability in also these parameters is the topic of an ongoing study conducted by the authors.

Fractured ribs remain one of the most common vehicle occupant injuries and detailed knowledge about the injury mechanism and contributing factors is lacking. The results of this study show that the variability in ribcage shape existing within a subpopulation of males influenced the predicted rib fracture risk in HBM simulations. Similar variability is likely to exist also in other subpopulations, such as average females, for example. As the ribcage shape of an occupant involved in a crash cannot be controlled for, this variability must be considered already in the design of the vehicle. Ensuring that the safety features of the vehicle are robust to the inherent human variability in ribcage shape can contribute to a reduction in rib fracture injuries in real-world crashes.

V. CONCLUSIONS

Two principal components, geometrically representing a variation in angles of the ribs (PC 1) and the length of the ribs (PC 2) in the ribcage explained more than 75% of the individual variability in ribcage shape in a subpopulation of close-to-average males.

Among PC-based ribcage variations, the variability in rib angles (PC 1) and rib lengths (PC 2) contributed the most to the variability in rib fracture risk predictions in both frontal and near side lateral impact.

HBM modelling methods aiming to represent human shape variability within the population of vehicle occupants should consider parametrisation beyond sex, age, height, and weight, to be able to represent the individual variations that influence occupant rib fracture risk.

VI. ACKNOWLEDGEMENT

The work performed in this study was funded by FFI-Strategic Vehicle Research and Innovation, by Vinnova, the Swedish Energy Agency, the Swedish Transport Administration and the Swedish vehicle industry.

The work was carried out at SAFER – Vehicle and Traffic Safety Centre at Chalmers, Sweden.

VII. REFERENCES

[1] Kullgren A, Stigson H, and Axelsson A. Developments in car crash safety since the 1980s, *Proceedings of IRCOBI Conference* 2020, Munich, Germany.

[2] Forman J, Poplin G. et al. Automobile injury trends in the contemporary fleet: Belted occupants in frontal collisions. *Traffic Injury Prevention*, 2019, vol. 20(6), pp. 607–612, doi: 10.1080/15389588.2019.1630825.

[3] Pipkorn B, Iraeus J, Lindkvist M, Puthan P, and Bunketorp O. Occupant injuries in light passenger vehicles—A NASS study to enable priorities for development of injury prediction capabilities of human body models. *Accident Analysis and Prevention*, 2020, vol. 138(105443), doi: 10.1016/j.aap.2020.105443.

[4] Bose D, Segui-Gomez M, Crandall J. R. Vulnerability of female drivers involved in motor vehicle crashes: An analysis of US population at risk. *American Journal of Public Health*, 2011, vol. 101(12), pp. 2368–2373, doi: 10.2105/AJPH.2011.300275.

[5] Carter P, Flannagan C, Reed M, Cunningham R, and Rupp J. Comparing the effects of age, BMI and gender on severe injury (AIS 3+) in motor-vehicle crashes. 2014, *Accident Analysis and Prevention*, vol. 72, pp. 146–160, doi: 10.1016/j.aap.2014.05.024.

[6] Shigeta K, Kitagawa Y, and Yasuki T. Development of next generation human FE-model capable of organ injury prediction. Paper No. 09-0111, 2009, *Proceedings of the 21st Enhanced Safety Vehicle (ESV) Conference*, Stuttgart, Germany.

[7] Gayzik F, Moreno D, Vavalle N, Rhyne A, and Stitzel J. Development of a Full Human Body Finite Element Model for Blunt Injury Prediction Utilizing a Multi-Modality Medical Imaging Protocol, 2012, *12th International LS-DYNA Users Conference*, Detroit, USA**.**

[8] Pipkorn B, Östh J, et al. Validation of the SAFER Human Body Model Kinematics in Far-Side Impacts, 2021, *Proceedings of IRCOBI Conference*, online conference.

[9] Pipkorn B, Iraeus J, Björklund M, Bunketorp O, and Jakobsson L. Multi-Scale Validation of a Rib Fracture Prediction Method for Human Body Models, 2019, *Proceedings of IRCOBI Conference*, Florence, Italy.

[10] Kent R, Lee S-H, et al. Structural and material changes in the aging thorax and their role in crash protection for older occupants, 2005, *Stapp Car Crash Journal*, vol. 49, pp. 231–249.

[11] El-Jawahri R, Laituri R, Ruan J, Rouhana S, and Barbat S. Development and Validation of Age-Dependent FE Human Models of a Mid-Sized Male Thorax, 2010, *Stapp Car Crash Journal*, vol. 54, pp. 407–430. doi: 10.4271/2010-22-0017.

[12] Schoell S, Weaver A, Vavalle N, and Stitzel J. Age- and Sex-Specific Thorax Finite Element Model Development and Simulation, 2015, *Traffic Injury Prevention*, vol. 16, pp. 57–65, doi: 10.1080/15389588.2015.1005208.

[13] Hwang E, Hallman J, Klein K, Rupp J, Reed M, Hu J. Rapid Development of Diverse Human Body Models for Crash Simulations through Mesh Morphing, 2016, *SAE Technical Paper 2016-01-1491*

[14] Hu J, Zhang K, Reed M, Wang J, Neal M, and Lin C. Frontal crash simulations using parametric human models representing a diverse population, 2019, *Traffic Injury Prevention*, vol. 20(sup1), pp. S97–S105, doi: 10.1080/15389588.2019.1581926.

[15] Wang Y, Cao L. et al. A parametric ribcage geometry model accounting for variations among the adult population, *Journal of Biomechanics*, 2016, vol. 49(13), pp. 2791–2798, doi: 10.1016/j.jbiomech.2016.06.020.

[16] Holcombe S, Wang S, and Grotberg J. The effect of age and demographics on rib shape, *Journal of Anatomy*, 2017, vol. 231(2), pp. 229–247, doi: 10.1111/joa.12632.

[17] Park B-K, Jones M, Ebert S, and Reed M. A parametric modeling of adult body shape in a supported seated posture including effects of age, 2021, *Ergonomics*, doi: 10.1080/00140139.2021.1992020.

[18] Klein K, Hu J, Reed M, Hoff C, and Rupp J. Development and Validation of Statistical Models of Femur Geometry for Use with Parametric Finite Element Models, *Annals of Biomedical Engineering*, 2015, vol. 43(10), pp. 2503–2514, doi: 10.1007/s10439-015-1307-6.

[19] Sobol' I. Global sensitivity indices for nonlinear mathematical models and their Monte Carlo estimates, *Mathematics and Computers in Simulation*, 2001, vol. 55, pp. 271–280, doi: 10.1016/S0378-4754(00)00270-6.

[20] Homma T and Saltelli A. Importance measures in global sensitivity analysis of nonlinear models, *Reliability Engineering & System Safety*, 1996, vol. 52, pp. 1–17, doi: 10.1016/0951-8320(96)00002-6.

[21] Iraeus J and Pipkorn B. Development and Validation of a Generic Finite Element Ribcage to be used for Strain-based Fracture Prediction, 2019, *Proceedings of IRCOBI Conference*, Florence, Italy.

[22] Iraeus J, Brolin K, and Pipkorn B. Generic finite element models of human ribs, developed and validated for stiffness and strain prediction – To be used in rib fracture risk evaluation for the human population in vehicle crashes, *Journal of the Mechanical Behavior of Biomedical Materials*, 2020, vol. 106(103742), doi: 10.1016/j.jmbbm.2020.103742.

[23] Iraeus J and Lindquist M. Development and validation of a generic finite element vehicle buck model for the analysis of driver rib fractures in real life nearside oblique frontal crashes, *Accident Analysis & Prevention*, 2016, vol. 95, pp. 42–56, doi: 10.1016/j.aap.2016.06.020.

[24] Zhang X and Pandey M. An effective approximation for variance-based global sensitivity analysis, *Reliability Engineering & System Safety*, 2014, vol. 121, pp. 164–174, doi: 10.1016/j.ress.2013.07.010.

[25] Forman J, Kent R, Mroz K, Pipkorn B, Bostrom O, and Segui-Gomez M. Predicting rib fracture risk with whole-body finite element models: development and preliminary evaluation of a probabilistic analytical framework. *Annals of Advances in Automotive Medicine*, 2012, vol. 56, pp. 109–124.

[26] Larsson K-J, Blennow A, Iraeus J, Pipkorn B, and Lubbe N. Rib Cortical Bone Fracture Risk as a Function of Age and Rib Strain: Updated Injury Prediction Using Finite Element Human Body Models, *Frontiers in Bioengineering and Biotechnology,* 2021, vol. 9, doi: 10.3389/fbioe.2021.677768.

[27] Holcombe S, Wang S, and Grotberg J, Modeling female and male rib geometry with logarithmic spirals, *Journal of Biomechanics*, 2016, vol. 49(13), pp. 2995–3003, doi: 10.1016/j.jbiomech.2016.07.021.

[28] Holcombe S, Wang S, and Grotberg J, Age-related changes in thoracic skeletal geometry of elderly females, *Traffic Injury Prevention*, 2017, vol. 18(S1), pp. S122–S128.

[29] Lee E, Craig M, and Scarboro M. Real-World Rib Fracture Patterns in Frontal Crashes in Different Restraint Conditions, *Traffic Injury Prevention*, 2015, vol. 16(sup2), pp. S115–S123 doi: 10.1080/15389588.2015.1062888.

[30] Liebsch C, Seiffert T, Vlcek M, Beer M, Huber-Lang M, and Wilke H-J. Patterns of serial rib fractures after blunt chest trauma: An analysis of 380 cases, *PLoS ONE*, 2019, vol. 14(12), doi: 10.1371/journal.pone.0224105.

[31] Folch-Fortuny A, Arteaga Moreno F J, and Ferrer Riquelme A J, PCA model building with missing data: New proposals and a comparative study, *Chemometrics and Intelligent Laboratory Systems*, 2015, vol. 146, pp. 77–88, doi: 10.1016/j.chemolab.2015.05.006.

[32] Folch-Fortuny A, Arteaga Moreno F J, and Ferrer Riquelme A J. Missing Data Imputation Toolbox for MATLAB, *Chemometrics and Intelligent Laboratory Systems*, 2016, vol. 154, pp. 93–100, doi: 10.1016/j.chemolab.2016.03.019.

[33] Shi X, Cao L, Reed M, Rupp J, Hoff C, and Hu J. A statistical human rib cage geometry model accounting for variations by age, sex, stature and body mass index, *Journal of Biomechanics*, 2014, vol. 47, no. 10, pp. 2277–2285, doi: 10.1016/j.jbiomech.2014.04.045.

[34] Sobol' I. On sensitivity estimation for nonlinear mathematical models, *Matem. Mod.*, 1990, vol. 2(1), pp. 112–118.

[35] Saltelli A, Ratto M, et al.. *Global sensitivity analysis: the primer*. Chichester, England ; Hoboken, NJ: John Wiley & Sons Ltd, 2008.

[36] Larsson K-J. Animations of PC-morphed SHBM, figshare, 2021, [Online]. Available: doi.org/10.6084/m9.figshare.17259014.v1

[37] Katzenberger M, Albert D, Agnew A, and Kemper A. Effects of sex, age, and two loading rates on the tensile material properties of human rib cortical bone, *Journal of the Mechanical Behavior of Biomedical Materials*, 2020, vol. 102(103410), doi: 10.1016/j.jmbbm.2019.103410.

[38] Velázquez-Ameijide J, García-Vilana S, et al. Influence of anthropometric variables on the mechanical properties of human rib cortical bone, 2021, *Biomed. Phys. Eng. Express*, vol. 7(3), doi: 10.1088/2057-1976/abf787.

[39] Agnew A, Murach M, et al. Sources of Variability in Structural Bending Response of Pediatric and Adult Human Ribs in Dynamic Frontal Impacts, *Stapp Car Crash Journal*, 2018, vol. 62, pp. 119–192.

[40] Holcombe S, Kang Y-S, Derstine B, Wang S, and Agnew A. Regional maps of rib cortical bone thickness and cross-sectional geometry, *Journal of Anatomy*, 2019, vol. 235(5), pp. 883–891 doi: 10.1111/joa.13045.

VIII. APPENDIX A. SUPPLEMENTARY MATERIAL

Descriptive statistics of the 89 males in the subpopulation are provided in TABLE A I.

TABLE A I
DESCRIPTIVE STATISTICS OF THE 89 MALES IN THE SUBPOPULATION

	Age [years]	Height [m]	Weight [kg]	BMI [kg/m^2]
Min	19	1.73	72	22.3
Median	50	1.75	77	24.8
Max	89	1.80	82	27.4
Num. Missing	16	-	-	-

The kinematics of the SHBM with the average ribcage shape is shown for the frontal impact and the near-side lateral impact in Fig. A 1.

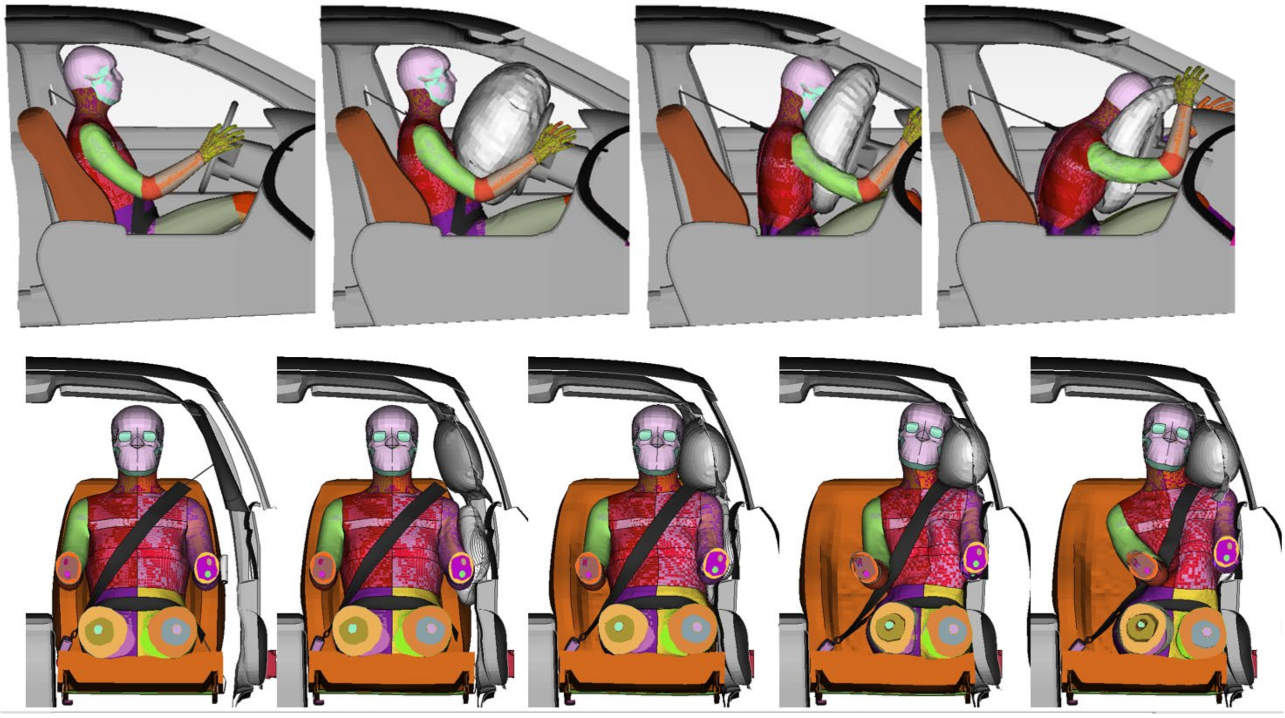

Fig. A 1. SHBM with average ribcage shape in the impact events. (Top) frontal impact at times (left to right) 0ms, 40ms, 80ms, and 120ms. (Bottom) lateral impact at times 0ms, 20ms, 40ms, 60ms, and 80ms.

TABLE A II shows the variance explained and the score SD for the first ten principal components.

TABLE A II
PCA RESULTS. PERCENT OF TOTAL VARIANCE EXPLAINED, CUMULATIVE SUM OF VARIANCE EXPLAINED, AND STANDARD DEVIATION OF SCORES IN THE SAMPLE FOR THE FIRST 10 PRINCIPAL COMPONENTS

Principal component	Variance explained [%]	Cumulative variance explained [%]	Score standard deviation
1	53.4	53.4	414.0
2	22.5	75.9	268.7
3	5.3	81.2	130.5
4	4.1	85.3	114.9
5	3.3	88.6	102.6
6	2.4	91.0	87.5
7	1.6	92.6	72.7
8	1.0	93.6	56.1
9	0.9	94.5	54.3
10	0.7	95.2	45.8

In Fig. A 2 the change in strain at time T=95ms, due to changing ribcage shape according to PC2 in the frontal impact is shown. For a ribcage with longer and less curved ribs (s=1.81), the strain increased in right side ribs (levels 5-9) and was decreased in left upper ribs (level 3-5).

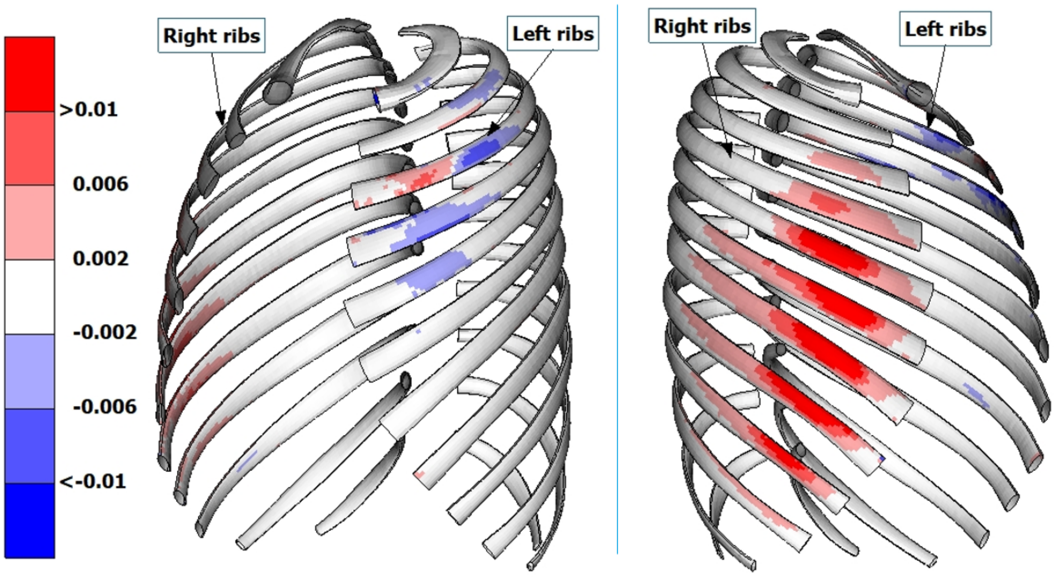

Fig. A 2 PC 2, Frontal Impact, time T=95 ms: difference in rib cortical bone first principal strain. Views of the ribcage focusing on left and right ribs. Strains from s=-1.81 ribcage shape elementwise subtracted from s=1.81 ribcage shape. Red means difference is positive, blue means negative by 0.01 (1%-unit)

Lateral impact NFR2+ risk plotted vs. maximum lateral ribcage width is shown in Fig. A 3.

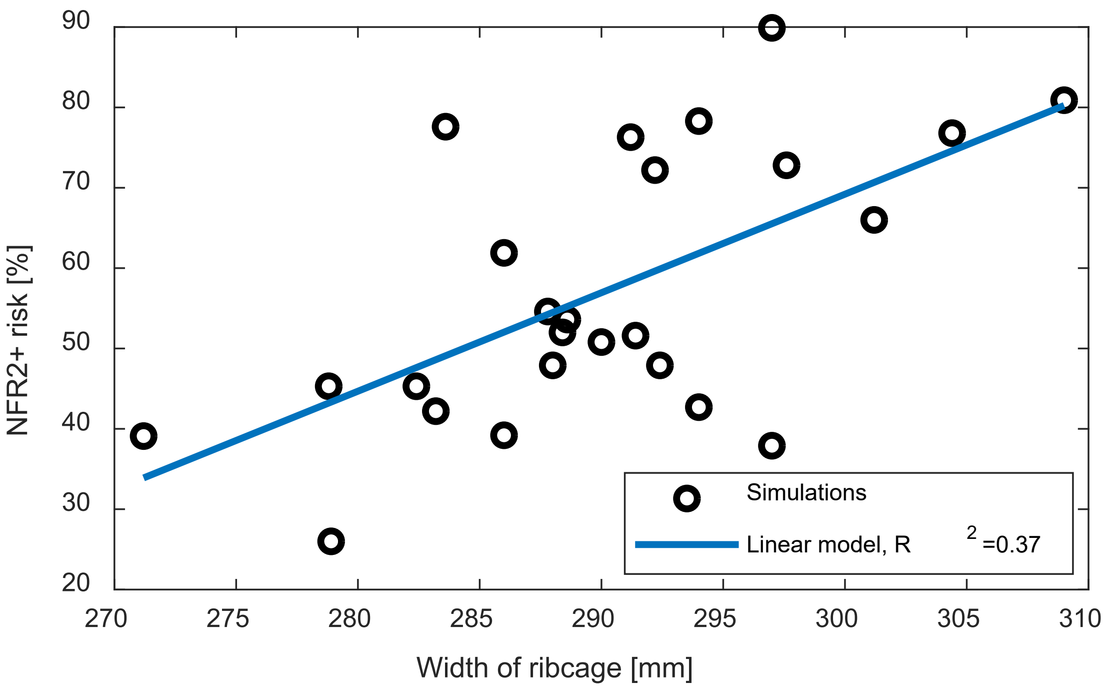

Fig. A 3 Lateral impact NFR2+ risk vs. maximum lateral width of ribcage for all evaluated ribcage shapes. Circles are simulation results, blue line is a linear model for NFR2+ as function of width, p=0.0012.

Figures demonstrating how the shoulder belt webbing was initially positioned relative to the varied ribcage shapes created using PC 1 (Fig. A 4) and PC 2 (Fig. A 5). For the ribcage shapes modified by both PCs, the superior edge of the shoulder belt webbing crosses the centre of the sternum at the level of the third rib pair.

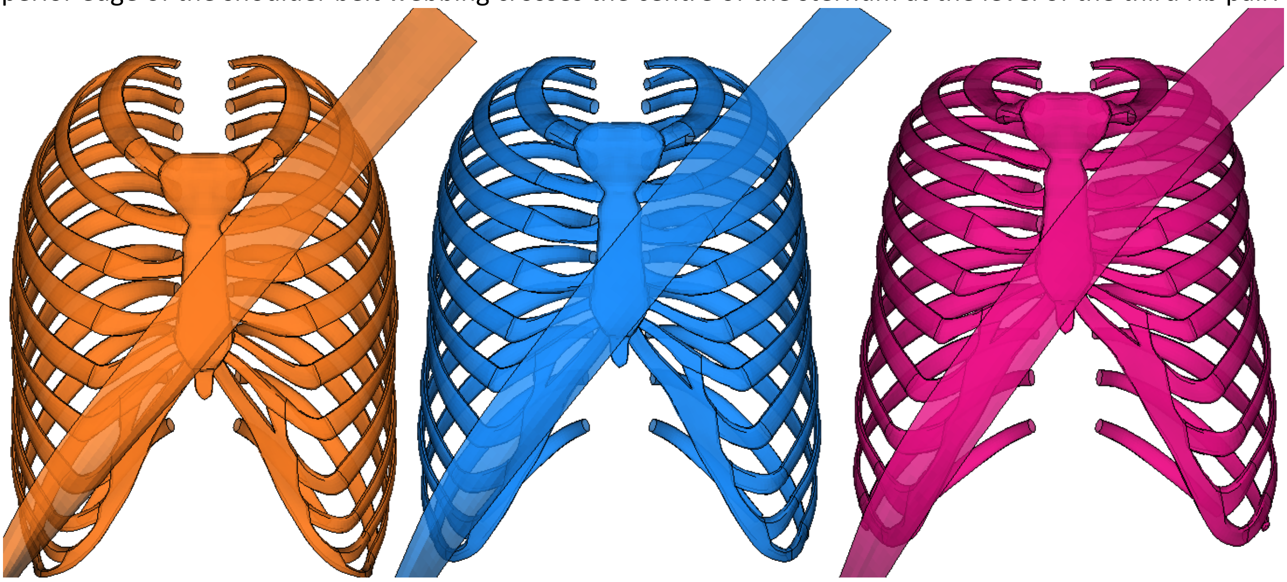

Fig. A 4 PC 1 variations of ribcage shape and the corresponding shoulder belt webbing. Left to right: s=-1.81, s=0, s=1.81

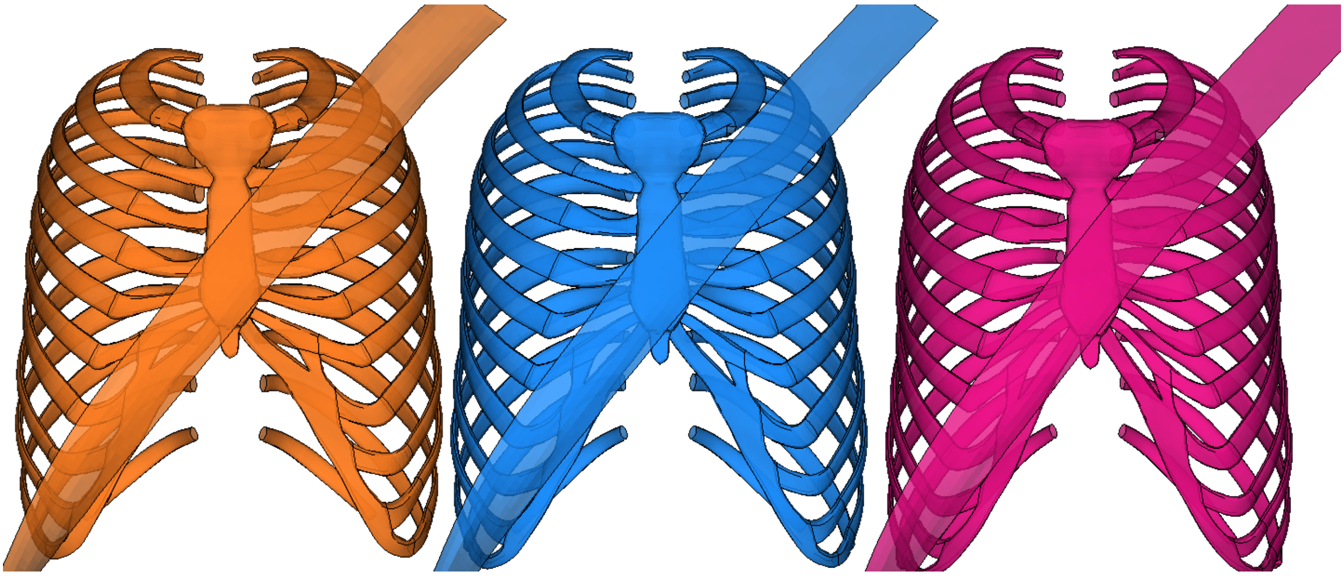

Fig. A 5 PC 2 variations of ribcage shape and the corresponding shoulder belt webbing. Left to right: s=-1.81, s=0, s=1.81